RESULTS FROM POINT CONTACT TUNNELING SPECTROSCOPY AND ATOMIC LAYER DEPOSITION*

Th. Proslier#, J. Norem, J. Elam, M. Pellin, Argonne National Laboratory, IL, U.S.A.
J. Zasadzinski, Illinois Institute of Technology, IL, U.S.A.
G. Ciovati, P. Kneisel, Jefferson Laboratory, VA, U.S.A.

Abstract

After decades of investigations, a complete and fundamental understanding of the dissipation and failure mechanisms of Superconducting RF cavities is still missing. In the first part of this paper we present recent studies of the superconducting properties measured by Point contact tunneling (PCT) spectroscopy at the surface of niobium coupons cut from cavity regions showing high (so-called Hot spots) and low (so-called cold spots) dissipation as inferred from thermometry measurement in the medium field Q-slope region. A comparison will be done with preliminary results obtained on an unbaked niobium coupon electropolished (EP). The second part is dedicated to Atomic layer deposition (ALD), from recent results of ALD- made superconductors to RF test of the post- annealing procedure on ALD-coated SRF cavities that was previously found to improve the superconducting properties of EP niobium coupons.

INVESTIGATION BY PCT OF THE SURFACE SUPERCONDUCTIVITY

Previous studies [1] by PCT spectroscopy of the surface superconductivity revealed a deviation from the ideal BCS superconductor and suggested magnetism and its effects on the superconducting density of states (DOS) underneath the oxides as a possible new dissipative mechanism in niobium cavities. The PCT results and the work of Cava [2] on defected $Nb_2O_{5-\delta}$ samples with a controlled concentration of oxygen vacancies shows that localized magnetic moments are present on the Nb4+ ions and give a possible origin of the magnetism that we observed. Besides, the results on mild-baked EP Nb coupons showed an improvement of the superconductivity as compared to an unbakedcoupons, in correlation with niobium cavities tests. This hypothesis have been recently supported by new results we obtained by PCT on niobium samples cut from regions of the niobium cavity walls that exhibits both anomalous and "normal" dissipative behaviour as deduced from thermometry measurements and further referred respectively as hot and cold spot samples. Three hot and three cold spots samples given by G. Ciovati from Jlab were cooled down to 1.6 K. On each sample tens of tunnel junctions have been measured in different places in order to insure that the results were reproducible and representative of a macroscopic behaviour.

We have categorized the conductance spectrum into two kinds. The first one is presented on figure 1, left, by three conductance spectrum that share common features: their shape is smeared as compared to the expected shape for an ideal BCS superconductor represented in red, in more details: the quasiparticles peaks are broadened and the value of the conductance at the Fermi level (bias V= 0 mV), so called the zero bias conductance or ZBC, is ranging between 0.02 and 0.75. The finite value of the ZBC indicates that quasiparticles are present at the Fermi level even at low temperature (1.6K). These unpaired electrons will couple to the external electromagnetic field ($B^2/8\pi$~μeV around the Fermi level) presents inside the cavity, and dissipate due to the finite normal metal resistivity where:

$$ZBC = \frac{N_{Super}(E_F)}{N_{Norm}(E_F)}, R_{Res} \propto N_{Super}(E_F)$$

Where, $N_{Super}(E_F)$ and $N_{Norm}(E_F)$ are respectively the superconducting and normal density of states at the Fermi level, R_{Res} is the residual resistance. This general result, always seen in cavity grade Nb samples (hot and cold spots), might explain the finite resistance, R_{res}, value measured on cavities at low temperature.

A second kind of spectrum is represented on figure 1, right in solid black line and is only seen on hot spots samples. They are characterized by values of the ZBC between 0.8 and 1.5, due mainly to a peak that appears at zero bias in between the two quasiparticle peaks at ±2 mV. We have artificially subtracted a conductance spectrum from the first kind that matches the quasiparticles peaks (in dashed line) and obtained a peak, in red, centred around the Fermi level. The peak obtained represents an additional tunneling channel and give a qualitative

*Work supported by DOE, office of Sciences under contract # DE-AC02-06CH11357
#proslier@anl.gov

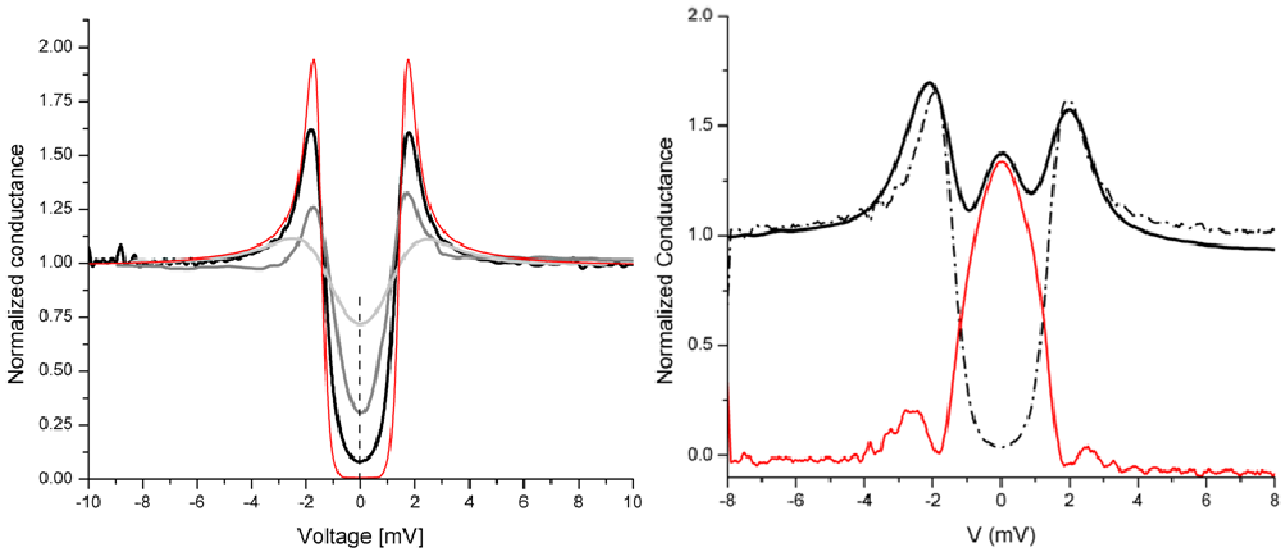

Figure 1: Conductance spectrum measured on Hot and cold spots samples. Left, spectrum of the first kind: in solid black line is a typical conductance curve measured on a cold spot samples, in gray and light gray measured on hot sot sample. Right, in solid black line a typical spectrum of the second kind measured only on hot spots samples. In dotted-dashed line a typical conductance curve from the first kind that matches the peaks amplitude. In red is the difference between the two.

idea of the conductance spectrum we would measure if the superconductivity were killed.

A statistic of the ZBC values measured on the 6 samples is represented in figure 2 left. The distribution of ZBC values for cold spots samples plot in solid lines, can be fitted by a Gaussian centers around 0.15 and of half width of 0.1. A typical spectrum is represented in solid dark line in figure 1 left, these spectrum are the closest we measured to an ideal superconductor. The fits with the Dynes- modified BCS theory (not shown) give values of the superconducting gap $1.5< \Delta< 1.55$ meV and pair breaking parameter $0.01< \Gamma<0.2$ meV. For hot spots however, a first peak in the distribution of ZBC values is centred around 0.3 with a half width of 0.2 in average. Typical spectrums are represented in gray and light gray in Figure 1 left and the fits give: $1.2<\Delta<1.55$ meV and $0.02< \Gamma<1$ meV. These lower values of the superconducting gap and higher values of the inelastic scattering parameter in average imply that the superconducting is degraded as compared to a cold sample and indicate that there is more unpaired electrons and therefore more dissipation in those samples.

A second peak in the distribution appears only in the hot spots samples at higher ZBC values and refers to the second kind of spectrum mentioned earlier (Figure 1 left). The microscopic origin of the ZBC peak can be unveiled by studying its temperature dependence. The latter shows a general trend: the ZBC peak appears at $T\leq 30$ K, increases in amplitude and gets narrower as the temperature decreases, as can be seen in Figure 2 upper right. For temperature below Tc=9.2 K, the superconductivity begins appearing and the quasiparticle peaks emerge from the broad background. Two effects compete then: the decrease of the density of states and the emergence of the growing ZBC peak at the Fermi level. To unravel the convolution of these two opposite effects, we applied a magnetic field H of 0.55 T above Hc2 of niobium (0.35 T) perpendicular to the sample at T>Tc and measured again the temperature dependence of the ZBC peak from 3 to 25 K (Figure 2 lower right).

The logarithmic dependence of the amplitude of the peak normalized to an extrapolated background ($G_O(E_f)$) is represented on Figure 3, and according to Appelbaum theory [3] is a characteristic signature of localized magnetic moments presents in the tunnel barrier, here the niobium oxides. The same dependence has been systematically observed for each ZBC peak measured.

The fits based on Appelbaum theory:

$$\frac{\Delta G(E_f)}{G_0(E_f)} = -4J(\rho_a + \rho_b)\times\ln(T/T_0)$$

Where $\Delta G(E_f) = G(E_f)-G_O(E_f)$, $\rho_{a,b}$ is the density of states of the two electrodes (gold tip and niobium) at the Fermi level and T_O is the closing temperature, gives always $J > 0$ with values that vary from junction to junction and a $T_O \sim 25$ K. Similar results have been obtained with Tantalum barrier by Watt [4] but the amplitude of the peak was much smaller (20%) as compared to our results (300 %). To our knowledge this is the first measurement of magnetic impurities into the niobium oxides by tunneling spectroscopy.

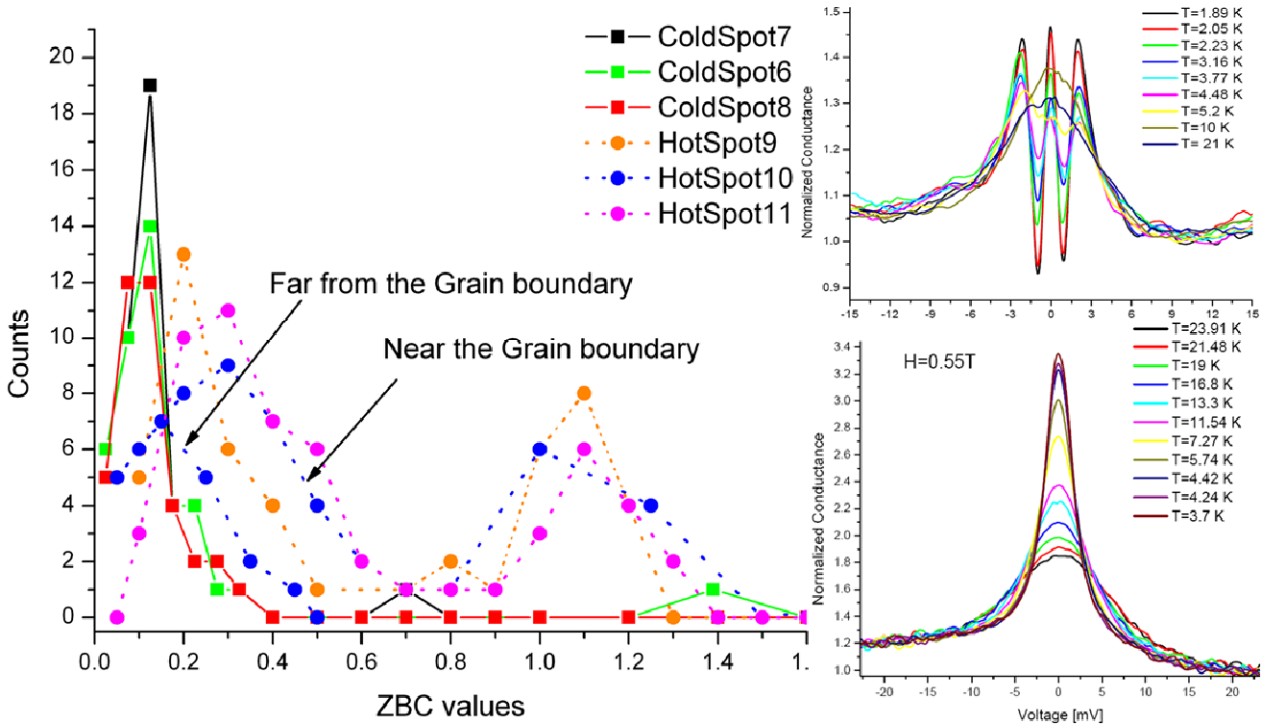

Figure 2: Left, statistic of the ZBC extracted from the conductance curves measured on hot and cold spot samples. Right, temperature dependence of a typical ZBC peak spectrum, Upper: coexisting with the superconductivity, Lower: a magnetic field of 0.55T has been applied to kill the superconductivity.

It is worth noticing that in the case of an ideal superconductor, there are no electrons present at the Fermi level, and therefore the ZBC magnetic peak could not be observed. Our hypothesis is that the magnetic impurities have a dual effect: the depairing of the surface superconductivity creates electron at the Fermi level that make possible the observation of the ZBC peak. Very recently and as preliminary results, we measured a splitting of the ZBC peak by a strong applied magnetic field applied perpendicular to the sample (not shown); the magnetic field dependence of the splitting value follow the Zeeman relation: $\Delta_H = g\,\mu_b H$ and is another proof that localized magnetic moments are present in the niobium oxides. The g-factor extrapolated from the linear fit give g~7 which suggest a strong orbital contribution to the total magnetic moment, in addition to the spin (g=2). Once again this is a preliminary results, the difficulty of such measurement resides in the instability of the junction with respect to high magnetic field, here up to 6T. To overcome this difficulty, smaller samples will be sent from Jlab and be measured by planar junction at Argonne in collaboration with U. Welp down to 3K and in magnetic field up to 9T. **However these results prove that magnetic impurities localized into the tunnel barrier are the origin of this ZBC peak.** Several questions are still open:

Why do these structures appear exclusively in hot spot samples?

What is the effect of the external RF magnetic field on the localized magnetic moments and how can they be added to simulation of Q(Eacc)?

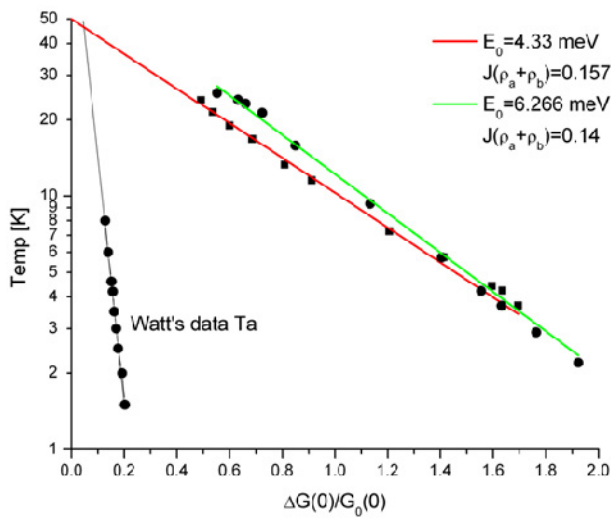

Figure 3: Temperature dependence of the normalized peak amplitude at 0 mV. The fits based on Appelbaum theory for two different junctions are represented on red and green. The Watt's data in black, measured on Tantalum barrier are here for comparison.

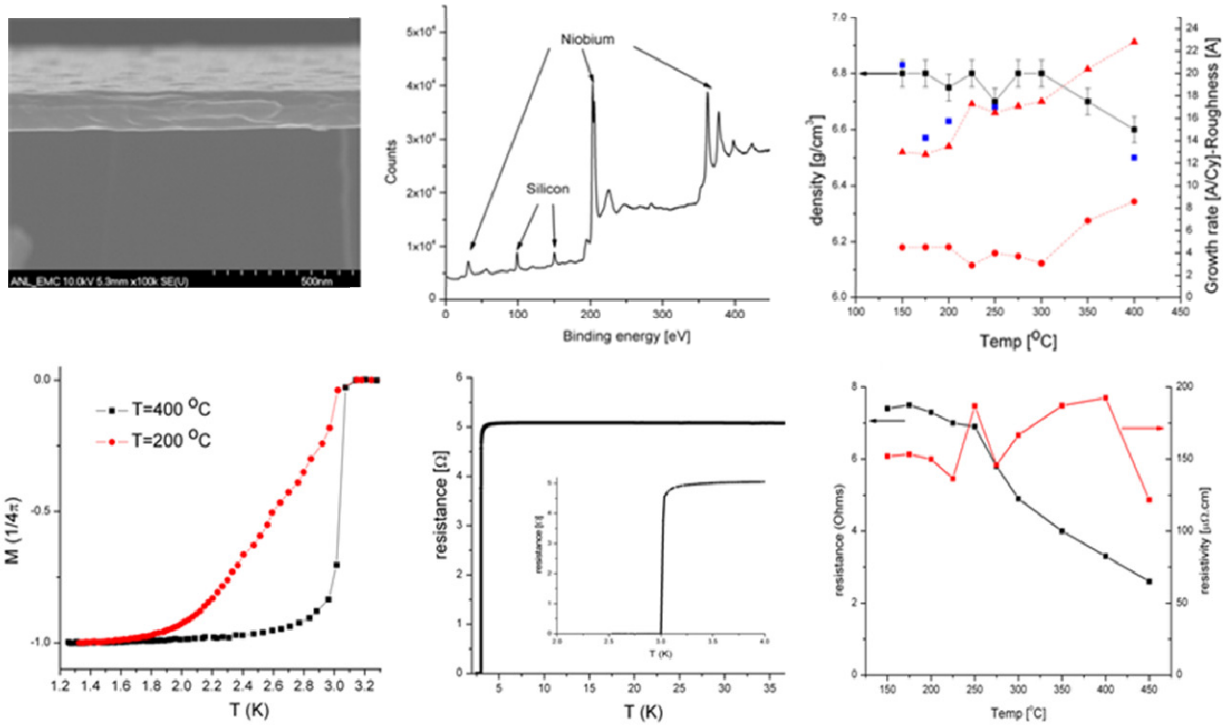

Figure 4: Typical ALD-made films characterization, from top to bottom, left to right: SEM, XPS, RBS and ellipsometry, SQUID, resistivity versus temperature, resistivity at room temperature.

ATOMIC LAYER DEPOSITION

The multilayer structure suggested by A. Gurevich [5] requires the growth of uniform films with good superconducting and metallic properties. This is our main challenge, as superconducting films made by ALD has never been studied. In a first part we will present the last results of our investigation of the growth condition of superconducting films by ALD. Prior to the deposition of the multilayers structure, the superconducting properties of the underneath niobium can be improved by an alumina ALD coating and a post annealing treatment in UHV, as shown on coupons. This process would constitute the first part of the multilayers synthesis by ALD and has been applied to 2 cavities RF cavities. The second part of this session is dedicated to the study of these results are presented.

Superconductors Made by ALD

We successfully synthesized various superconductors made by thermal ALD: NbN, TiN and NbSi. The NbN, of particular interest for the multilayer structure have been grown following the chemical reaction: $NbCl_5 + NH_3 = NbN + HCl$. The growth rate is found to be 0.3 Å/cycle, the Tc of the 100 nm thick film grown on Si (100) at 450°C was 5.5 K and the room temperature resistivity, ρ=400 μΩ.cm as compared to 200 μΩ.cm for ideal sputtered NbN films with a Tc of 16 K. We studied by XPS and in-situ sputtering the concentration of impurities in those films as a function of the growth temperature from 350 °C to 500°C and found that Cl is the main contaminant, ranging between 15% at 350 °C and 5% at 500 °C. The grain size for a 100 nm film is between 10 nm and 50 nm. As th quality of these films were poor, we investigate a new precursor: NbF5, the chemical reaction being very similar to the NbCl5 one. Similar results have been obtained and no significant improvement over the $NbCl_5$ precursors. In Both cases, the major problem of our films is the contamination of Cl or F that deteriorate significantly the normal and superconducting properties of the of NbN films. The addition of a chemical compound with a strong affinity with the Cl for instance, would help improving the film quality. We found that the addition of Zn vapour following the reaction: $NbCl_5 + Zn + NH_3 = NbN + ZnCl_2 + HCl$ decreases dramatically the Cl concentration in our NbN films by a factor of 5, ranging from 3% at 400C to less than 1% at 500C. The room temperature resistivity of a 10 nm thick film is found to be 220 μΩ.cm, for a growth rate of 0.25 Å/cy. We expect the resistivity of the films to further decrease for thicker films, as observed in all metallic alloys grown by ALD; using the same technique, Ritala [6] measured a value of ρ=200μΩ.cm for a 100 nm films, which correspond to 4000 cycles. The superconducting properties will be measured soon and we expect a Tc > 10 K. we will as well investigate the growth of ALD NbN on various substrates found, by sputtering, to have a good lattice match with NbN such as R-plan Sapphire.

We tried, in parallel to grow Nb metal by ALD with a method inspired from the previous work based on the chemical reaction: $WF_6 + Si_2H_6 = W + SiHF_3 + H_2$, replacing the WF_6 by NbF_5. The ALD regime of such reaction is limited to growth temperature below 200°C as the disilane decomposed above that, causing CVD. It turns out however that the most stable reaction product is NbSi when synthesized on Si (100) substrate, the same in the ALD or CVD regime: from 125 °C to 400 °C; in both case the presence of F impurities is undetectable by RBS (Rutherford back scattering). A systematic characterization of the chemical composition (RBS and XPS), roughness, resistivity and films morphology etc...is summarized on figure 5. To our surprise, the magnetization measurement by SQUID showed a superconducting transition at 3.1 K. The homogeneity of the superconducting properties, characterized by the sharpness of the transition can be significantly improved by increasing the growth temperature.

The secondary electron yield of NbSi is very low: up to 1.5 at 150 V and is extremely resistant to oxidation up to 1000 °C and to chemical corrosion. It could be used as a protective layer, on top of the last superconducting layer.

Interestingly, the same growth parameter leads to the synthesis of Nb_3Si_5 on Quartz substrate and to $NbSi_2$ on MgO. Both of them are not superconducting and the temperature dependence of the film's resistivity evolve from a quasi metallic (RRR=1) to an insulating behaviour as the concentration of Silicon increases. This is the first time, to our knowledge, that the film stoichiometry is influenced significantly by the interaction substrate-film. The elastic stress induced by the lattice mismatch allows the control of the growth phase, the goal being to grow Nb_3Si, an A-15 compound with a Tc of 18K. We are studying the chemical composition of films grown on other substrate such as R or A or C-plan sapphire growth that are the closest match to the Nb_3Si lattice parameter. This in-depth study and methodology of the optimal growth condition of Nb_3Si is a frame for others very similar A-15 such as Nb_3Ge that would be grown by $NbF_5 + Ge_2H_6 = NbGe$ + reaction products.

The films were synthesized by thermal ALD; we are in the process of buying a plasma ALD system with a delivering delay of 8 week, before Christmas we will grow the first layers of superconducting NbN. The Nb growth by PEALD is straightforward and very similar to other very reactive metals such a Titanium and Aluminium already grown by PEALD and based on the reactions: $TiCl_4 + H_2$-plasma = Ti + HCl or $AlCl_3 + H_2$-plasma etc... This new method will also allow much more flexibility for alloys growth. For instance, instead of relying on the more stable reaction product between two precursors, we could build an alloy by growing separately each of its components. For Nb_3Al (Tc=20K) we will grow 3 layers of Nb and one of Al. Besides, the metallic properties are much better with the plasma enhanced growth owing to a negligible level of impurities in the films: Ti, Ta, Cu and Al have resistivities around 10 μΩ.cm, very close to the bulk values. We will start with the PEALD growth study of NbN following the chemical reaction: $NbCl_5 + NH_3+H_2$-plasma = NbN + HCl, which occurs at much lower temperature (~200°C instead of 450°C) than the thermal ALD.

ALD Results on SRF Cavities: The Post Annealing Treatment at High Temperature (HT).

So far, three SRF cavities provided by J-lab have been ALD coated and tested. Two of them have been subsequently baked at high temperature 450°C in UHV for 20 hrs, following the same recipe found to improve the superconducting properties on niobium coupons [7]. The cavity one (not shown here) was previously coated by 10 nm of Al_2O_3 + 5 nm of Nb_2O_5, sent to J-lab, high pressure rinsed, tested then baked in UHV, high pressure rinsed and tested. After the HT baking, the maximum acceleration field E_{max} was reduced from 32MV/m down to 21 MV/m at which gradient the Q-factor dropped because of field emission of quenched.

The quality factor however was unchanged (1.10^{10}). These last results suggested that the quality of the oxides might have changed after the HT annealing. A densification of the ALD oxides layer has already been observed which would mean that the Secondary electron yield (SEY) of the layer increases too, causing the observed field emission. Another possible reason is cracks appearing in the protectives ALD layers due to thermal constraints during the temperature cycling. These cracks would then act as easy points of entry for oxygen-water during the subsequent HPR. Once the threshold is reached, irreversible damaged are caused to the 20 nm thick oxide layer.

In order to determine the origin of this degradation, we coated a second cavity with just 10 nm of Alumina at low temperature 90°C for 2 hrs, send it back to J-lab, HPR then tested (yellow points Figure 5 left). No multipacting occurred and the cavity performances were the same as the baseline (pink points Figure 5 left). The cavity was then HT baked, HPR and retested (black points) and the cavity quenched at the same field as cavity 1: E_{max} of 20 MV/m, but this time no field emission was measured. This result tends to support the quenching hypothesis observed after HT bake of cavity 1, and therefore the field emission hypothesis can be ruled out. The deterioration of the E_{max} but not of the Q-factor indicates that a contamination of the Nb at the interface with the oxides occurred during the HPR.

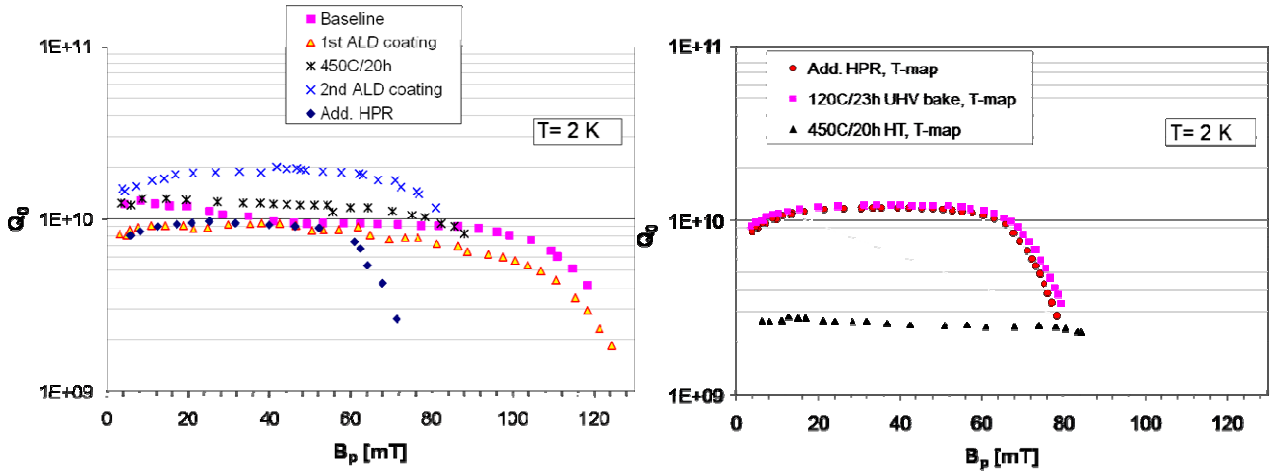

Figure 5: RF test of high temperature baked Nb cavity. Left, cavity 3 with a initial ALD coating of 10 nm Al_2O_3 and 5 nm Nb_2O_5 (red), then HT baked (green). Right, baseline (blue) followed by an initial ALD coating of 10 nm Al_2O_3(red), then HT baked (green), and finally re-coated by 10 nm of Al_2O_3 and 10 nm of Nb_2O_5 (black).

However, the contaminant (most likely oxygen) is probably localized otherwise the global cavity Q-factor would have been affected too. We synthesized a second ALD coating of 10 nm Al_2O_3 and 5 nm Nb_2O_5 (blue crosses Figure 5 left) at 250° C for 4 hrs and the cavity was tested back at J-lab; the quality factor increased by a factor of 2 but the E_{max} remained unchanged. It is interesting to note that an additional dielectric layer should not affect the underneath superconductivity, unless the higher deposition temperature removed part of the oxygen contamination present after the first HT baking. Besides, it has been found previously that baking the cavity at temperature higher than 145°C for few hours degraded the Q and the E_{max} [8], whereas here, the Q-factor increased! This raises an interesting question: How the last dielectric layer alone influences the Q-factor ad E_{max} of cavities? An additional HPR (in dark blue diamonds on Figure 5 left) induces a high field Q-slope that cannot be recovered after a 120°C baked (Figure 5 right in pink). A second HT baking at 450°C for 20 hrs decreases significantly the Q-factor but suppressed the high field Q-slope (in black Figure 5 right.).

To understand these last results, temperature maps have been measured (Figure 6 upper left and right respectively) before and after the second HT baking as a function of the amplitude of the magnetic field. Prior to the second HT baking, the temperature dependence has an exponential dependence (not shown) whereas after the dependence if quadratic indicative of Ohmic losses. Besides, the amplitude of ΔT is more homogenous and is twice smaller after the HT baking. That confirms both that the high field Q-slope is due to local hot spots and that the Q decrease is due to a massive injection of oxygen into a depth of at least ξ from the surface.

The averaged superconducting parameters extracted from the BCS fits of the surface resistance's temperature dependence, Rs[T], (Figure 6 middle, left) reveal however an improvement of the superconductivity: both Δ/kTc and the mean free path, l, increase, which means that the superconducting Nb that is not already contaminated have better characteristics.

In conclusion, we have now a better understanding of the HT baking effect on the cavity performance: each sequence HT+ HPR injects oxygen locally through cracks present in the ALD dielectric layers after the thermal cycling and diffuse from there, contaminating more Nb at each cycle HT+HPR. To prevent post contamination by HPR, the ideal would be to bake at High temperature inside a build-in cavity-ALD oven and recoat to fill the cracks, prior to exposing the cavity to air and any HPR. A measurement of the cracks density as a function of the dielectric layer is in progress at Argonne. It is important to note that the HT treatments on coupons test that showed an improvement of the superconductivity were not HPR. It would be interesting to measure again the same coupons after a few months exposure to air of water by PCT before and after and other HT baking.

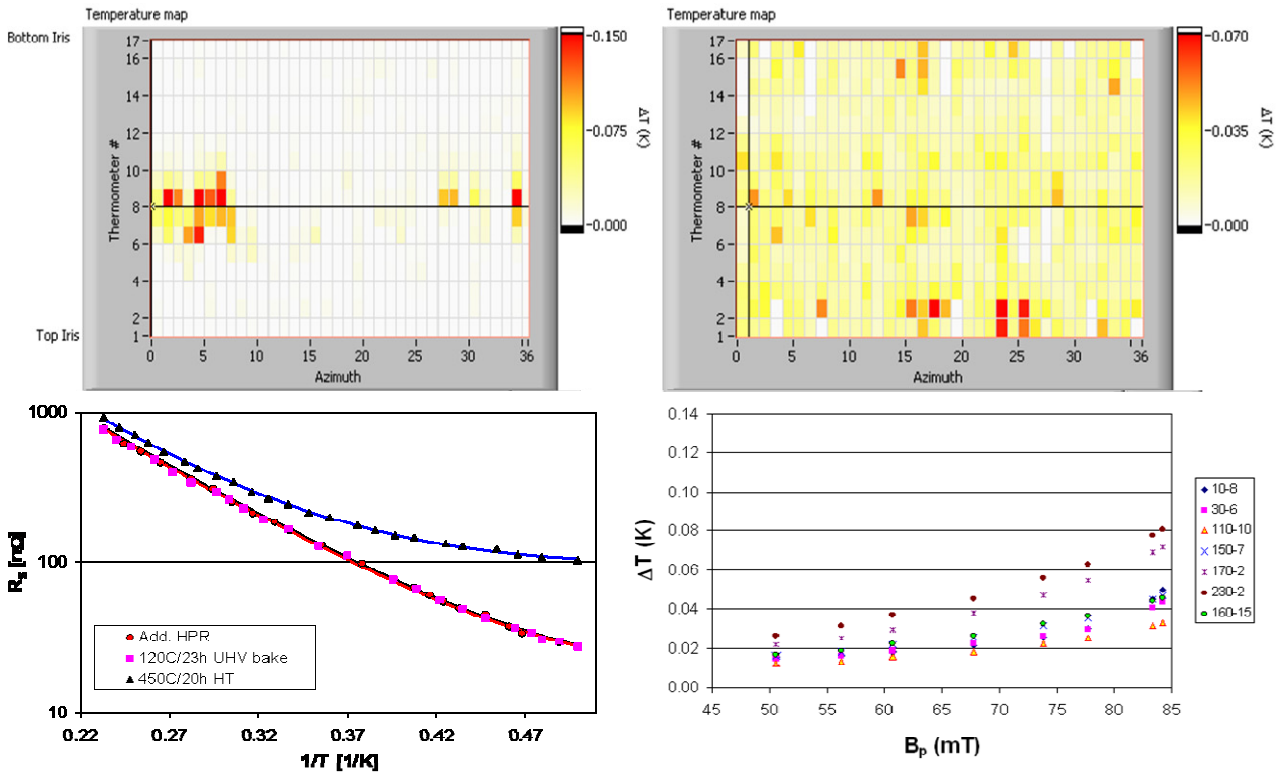

Treatment	Δ/kT_c	ℓ (nm)	R_{res} (nΩ)
Add. HPR	1.866 ± 0.018	19 ± 44	16.0 ± 0.8
120 °C/23 h bake	1.879 ± 0.005	18 ± 55	16.3 ± 0.5
450 °C/20 h HT	1.911 ± 0.026	58 ± 17	93.8 ± 0.2

Figure 6: Up, temperature maps at the highest magnetic field before (left) and after (right) HT baking. Middle, measurement of the temperature dependence of the average surface resistance of the cavity before and after HT baking (left). Thermometry measurements in few spots of ΔT as a function of the amplitude of applied magnetic field. Bottom, superconducting parameters extracted from the BCS fits of Rs(T).

REFERENCES

[1] Th. Proslier, J. Zasadzinski, M. Pellin, J. Norem et al APL 92, 212505 (2008).
[2] R. J. Cava, B. Batlogg, J. J. Krajewski et al, Nature 350, 598 (1991).
[3] J. Appelbaum. PRL 17, 91 (1966).
[4] A. F. G. Watts. PRL 13, 401 (1964).
[5] A. Gurevich. APL 88, 012511 (2006).
[6] K. E. Elers, M. Ritala, A. Surf. Sci 82, 468 (1994).
[7] Th. Proslier, J. Zasadzinski, J. Elam et al. APL 93, 192504 (2008).
[8] G. Ciovati, P. Kneisel and A. Gurevich. PR-ST AB 10, 062002 (2007).